Prospect of quantum anomalous Hall and quantum spin Hall effect in doped kagome lattice Mott insulators

Daniel Guterding,* Harald O. Jeschke, and Roser Valentí
Institut für Theoretische Physik, Goethe-Universität Frankfurt, Max-von-Laue-Straße 1, 60438 Frankfurt am Main, Germany

Electronic states with non-trivial topology host a number of novel phenomena with potential for revolutionizing information technology. The quantum anomalous Hall effect provides spin-polarized dissipation-free transport of electrons, while the quantum spin Hall effect in combination with superconductivity has been proposed as the basis for realizing decoherence-free quantum computing. We introduce a new strategy for realizing these effects, namely by hole and electron doping kagome lattice Mott insulators through, for instance, chemical substitution. As an example, we apply this new approach to the natural mineral herbertsmithite. We prove the feasibility of the proposed modifications by performing *ab-initio* density functional theory calculations and demonstrate the occurrence of the predicted effects using realistic models. Our results herald a new family of quantum anomalous Hall and quantum spin Hall insulators at affordable energy/temperature scales based on kagome lattices of transition metal ions.

PACS numbers: 71.20.-b, 73.43.-f, 75.10.Jm, 75.30.Et

arXiv:1511.05686v3 [cond-mat.mes-hall] 17 May 2016

INTRODUCTION

The kagome lattice structure, which consists of corner-sharing triangles, is notorious for supporting exotic states of matter. For instance, the possible experimental realization of quantum spin-liquids based on spin-1/2 kagome lattices has generated in the past intense research efforts on herbertsmithite and similar frustrated antiferromagnets [1–12]. Recently, the kagome lattice has also received plenty of attention for quasiparticle excitations with non-trivial topology [13–15]. From topologically non-trivial electronic bands, effects such as the quantum spin Hall effect (QSHE) [16–18] and the quantum anomalous Hall effect (QAHE) [19, 20] can emerge, also in kagome lattices [21, 22]. A quantum spin Hall insulator in two dimensions, also known as a topological insulator, is a topological state of matter, present in a system with spin-orbit coupling, where symmetry protected dissipationless spin-polarized currents counterpropagate on the sample edges, while the bulk of the sample remains insulating (Fig. 1a). This phenomenon has received considerable attention because Majorana bound states have been predicted to appear at interfaces between QSHE materials and superconductors [18, 23, 24]. Employing these Majorana zero modes for topological quantum computation is a rapidly developing field [25].

In contrast to the QSHE, in a quantum anomalous Hall insulator only one spin species propagates around the sample edge due to the presence of intrinsic magnetization in the sample (Fig. 1b). This state of matter offers a direct realization of *intrinsic* topological properties in a material through the combination of spin-orbit coupling and magnetism [17]. Due to the dissipation-free, spin-polarized edge currents in the absence of external magnetic fields, realizations of the QAHE are also intensively sought for, especially for application in new energy-efficient spintronic devices [26, 27]. So far, in electronic systems the QAHE has only been observed in thin films of chromium-doped $(Bi,Sb)_2Te_3$ at a temperature of 30 mK [28, 29], the main limitation being the low Curie temperature of the material involved. Lately, it has been proposed that the QAHE can be realized in some other compounds using, for instance, manipulated surfaces or exfoliated monolayers [30–32]. Another interesting approach is design from scratch of organometallic networks with topological bandstructures [33, 34]. A good strategy for designing QAHE compounds based on existing materials with favorable energy scales that are adequate for applications is however currently lacking.

Here, we propose a new approach to create materials with non-trivial band topology and large Curie temperatures, exploiting the electronic properties of doped Mott insulators on a kagome lattice. A quick look at the one-electron properties (bandstructure) of the kagome lattice with nearest neighbor hoppings (Fig. 2) shows huge potential for the realization of possible exotic states by only varying the electron filling. At half-filling the Fermi level lies near a van Hove singularity and inclusion of many-body correlation effects renders the system a Mott insulator [35]. At a filling of $n = 4/3$, however, the Mott transition is absent [12] and the Fermi level is at the Dirac point, where non-trivial band effects may be expected upon consideration of spin-orbit coupling. The spin-orbit coupling opens a gap at the position of the Dirac point and the non-trivial topology of electrons on the kagome lattice leads to surface states of both spin species that traverse the bulk band gap opened by relativistic effects and, the QSHE is realized.

Even more interesting is the filling of $n = 2/3$ with the Fermi level right at the flat band. It was recently suggested [36] that if a nearly flat band is partially filled, a proper combination of spin-orbit coupling, ferromag-

* guterding@itp.uni-frankfurt.de

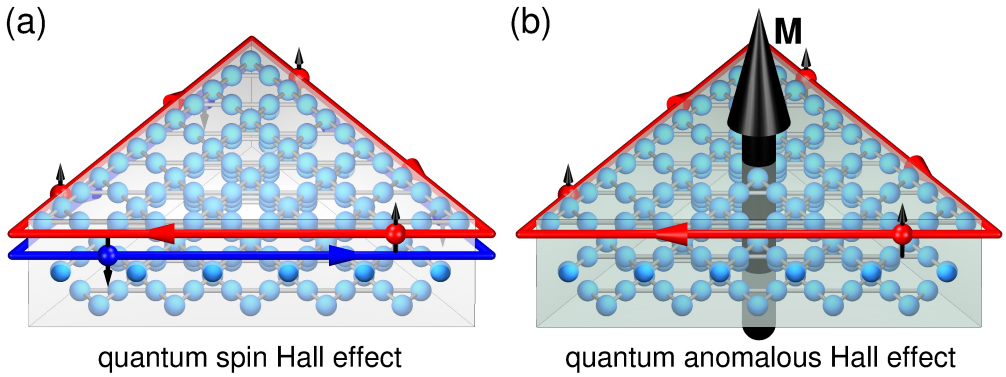

FIG. 1. Predicted quantum Hall effects in doped herbertsmithite. (a) Quantum spin Hall effect (QSHE) with counterpropagating edge currents of opposite spin-polarization. (b) Quantum anomalous Hall effect (QAHE) with a single spin-polarized edge current due to intrinsic magnetization. In both cases the crystal is cut into triangular shape. The crystal structure shows the arrangement of copper atoms (light blue balls) in three shifted kagome planes as in herbertsmithite.

netism and geometric frustration will give rise to the fractional quantum Hall effect at high temperatures. Along these lines, we exploit here as a key ingredient for topological non-trivial states, the tendency towards ferromagnetism [37] of a filled flat band in hole-doped transition-metal-based kagome lattices. At $n = 2/3$ the ferromagnetic instability combined with correlation effects is expected to gap out one spin-channel and move the Fermi level of the other spin-channel exactly to the Dirac point. When spin-orbit coupling (SOC) is considered, we have the same situation as for the filling of $n = 4/3$ but only for one spin species. In such a situation, the QAHE with fully spin-polarized dissipation-free surface states is realized.

To demonstrate this new strategy of finding QSHE and QAHE materials by doping Mott insulators, we investigate which possible modifications of the natural mineral herbertsmithite -a Mott insulator with spin-liquid behavior- leave the perfect kagome motif undistorted and realize different electronic fillings.

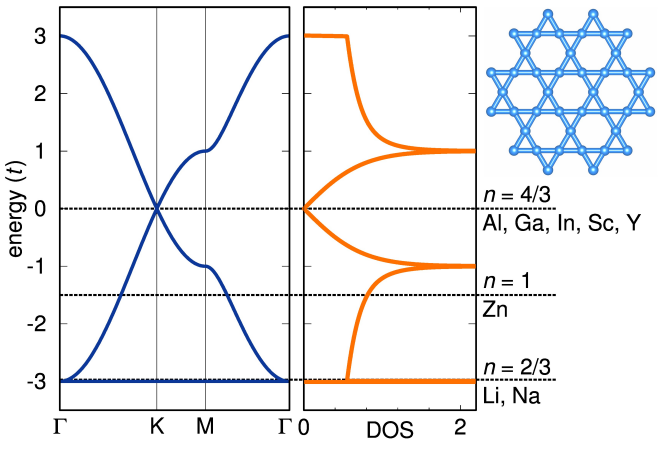

FIG. 2. Electronic bandstructure and density of states of the pure kagome lattice (shown in upper right corner). On the right hand side the possible substituent elements for the herbertsmithite system with corresponding Fermi level are listed.

Herbertsmithite crystallizes in the centrosymmetric space group $R\bar{3}m$ and its structure is based on layers of Cu^{2+} ($3d^9$) ions building a perfect two-dimensional half-filled frustrated kagome lattice separated by layers of Zn^{2+} ions (Fig. 3a). The Cu atoms are in a square planar crystal field environment of oxygen ions so that the orbitals near the Fermi level are correlated $d_{x^2-y^2}$ states. Evaluating density functional theory (DFT) total energies, we show that single crystals of materials obtained by following various doping choices in herbertsmithite can in principle be synthesized. Further, we prove that the magnetic ground state of hole-doped herbertsmithite at filling 2/3 is ferromagnetic, which validates that the flat band physics of the pure kagome lattice carries over to realistic situations. Finally, we demonstrate the presence of topologically non-trivial surface states of doped herbertsmithite using a state-of-the-art Wannier function technique based on fully relativistic DFT calculations.

MATERIALS AND METHODS

We prepared hypothetical materials starting from the experimental crystal structure of herbertsmithite [1], substituting zinc (Zn^{2+}) atoms between the copper kagome layers (see Fig. 3) by monovalent A=Li^+, Na^+ (hole-doping) and trivalent Al^{3+}, Ga^{3+}, In^{3+}, Sc^{3+}, Y^{3+} (electron-doping). We refer to these compounds as A-herbertsmithite, $ACu_3(OH)_6Cl_2$.

Experimental and hypothetical crystal structures were fully relaxed using DFT in the projector augmented wave (PAW) formulation [38] implemented in GPAW [39] with a plane-wave cutoff of 1000 eV and the GGA exchange-correlation functional [40]. We optimized the stoichiometric structures using 6^3 k-points (4^3 k-points for non-stoichiometric structures) until forces were below

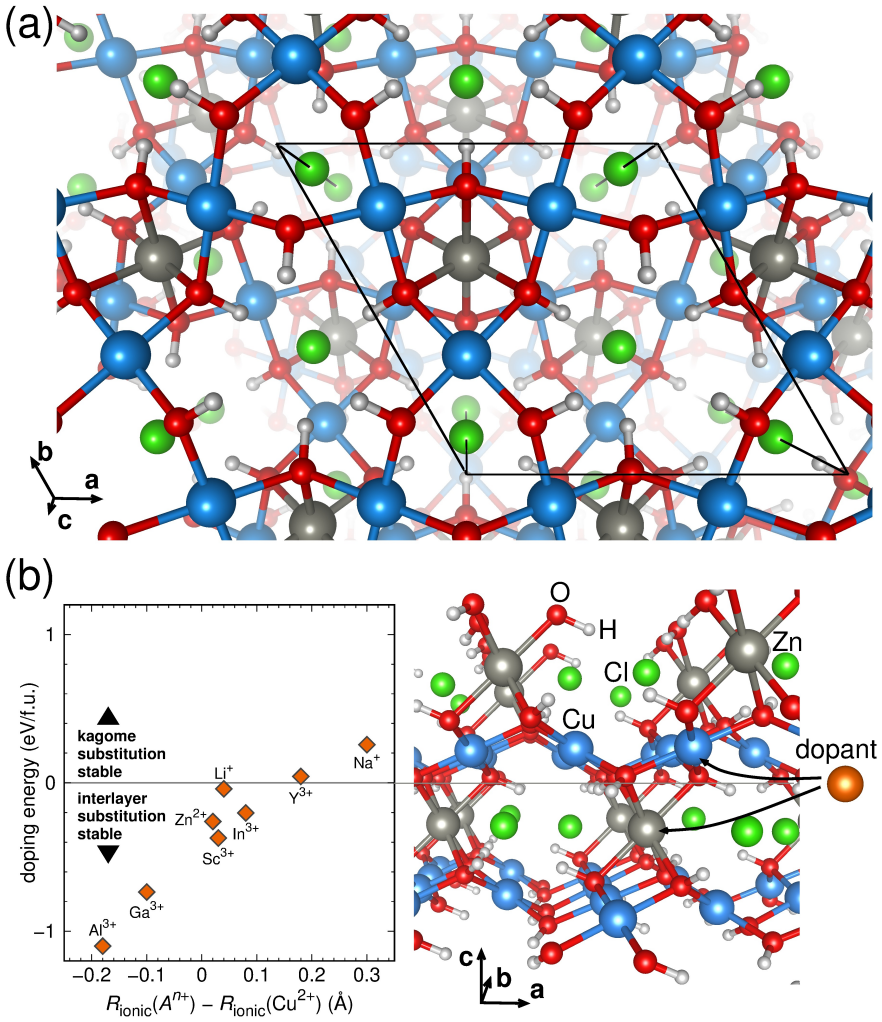

FIG. 3. Crystal structure and calculated doping energies for herbertsmithite. (a) View of the crystal structure of herbertsmithite along the c-axis, which is perpendicular to the copper kagome layers. The Cu atoms (shown in light blue) are in a square planar crystal field environment of oxygen ions (red) so that the orbitals near the Fermi level are correlated $d_{x^2-y^2}$ states. Each oxygen atom bonds to a hydrogen atom (white) located outside the copper and oxygen layer. In this interlayer space also zinc (grey) and chlorine (green) atoms are located. (b) The left hand side shows doping energies for herbertsmithite. All data points above the zero energy line indicate that the kagome lattice will be distorted upon doping. The right hand side shows the crystal structure of herbertsmithite with two possible sites for substitution indicated. On the interlayer site (Zn position, negative doping energy), herbertsmithite mostly prefers to incorporate ions with smaller radius than Cu^{2+}. All ions with positive doping energy occupy the Cu position and distort the kagome lattice. Ionic radii in coordination number 6 are taken from Ref. [47].

10 meV/Å.

For each of the substituted structures with perfect copper kagome layer we also constructed a defect structure, where we lowered the symmetry of the unit cell and exchanged the substituent A with a copper atom from a kagome lattice site. As the chemical composition of these defect structures is identical to the defect-free structures, energy differences can be evaluated directly within DFT. In case the defect structure has lower energy, the kagome lattice is likely to be destroyed and the phenomena of interest here will not arise in the target compound.

Total energies, electronic bandstructures and magnetic exchange interactions of the relaxed structures were then evaluated using *ab-initio* DFT calculations within an all-electron full-potential local orbital (FPLO) [41] basis. For the exchange-correlation functional we employed the generalized gradient approximation (GGA) [40], as well as DFT+U [42] functionals. The latter was necessary in order to treat the correlated nature of Cu 3d orbitals. The Hubbard repulsion on the Cu 3d orbitals was set to $U = 6$ eV and Hund's rule coupling to $J_H = 1$ eV. Although we concentrate our investigation on the Cu $d_{x^2-y^2}$ orbitals close to the Fermi level, the interactions were included in the entire Cu 3d shell, which is spread out over a large range of energies due to the interaction with the ligands. Additionally, we investigated the effect of

spin-orbit coupling on the electronic bandstructure employing the fully relativistic version of the FPLO code. Total energies, electronic bandstructures, tight-binding and Heisenberg models were extracted from calculations converged using 8^3, 20^3, 40^3 and 6^3 k-point grids respectively.

To demonstrate the existence of surface states, we constructed bulk tight-binding models for the copper states $(n, j, m_j) = (3, 5/2, \pm 5/2)$ from fully relativistic DFT calculations using projective Wannier functions [43]. Employing a method based on Green's functions [44–46], we calculate the states on the surface of herbertsmithite. The spectral function is obtained from the Green's function as $A(k,\omega) = -\mathrm{Im}\, G(k,\omega)/\pi$.

RESULTS

Stability estimates

By performing exhaustive DFT calculations we identified as the limiting factor for modifying herbertsmithite the tendency of certain ions towards substituting copper sites in the kagome layer. In Fig. 3b we plot the energy difference (tabulated in the Supplemental Information) between substitution at the kagome site and substitution at the interlayer site for herbertsmithite as a function of the substituent ionic radius [47]. In herbertsmithite, sodium (Na^+) and yttrium (Y^{3+}) prefer to occupy a site in the kagome layer, which generates a monoclinically distorted crystal structure with no perfect kagome lattice. If the substituent atom occupies the interlayer site, the perfect kagome motif is preserved.

In terms of substitution energies, lithium (Li^+) is the most promising candidate for synthesis of hole-doped herbertsmithite. On the electron-doped side, aluminum (Al^{3+}), gallium (Ga^{3+}) and scandium (Sc^{3+}) are the most promising candidates for substitution. Formation of the substituted materials is found to be energetically favorable compared to the formation of the parent compound clinoatacamite, $Cu_2(OH)_3Cl$. All herbertsmithite-based materials investigated are stable against formation of vacancies and copper impurities, as opposed to full substitution, on the interlayer site. We also investigated fractional substitution of Zn^{2+} by Ga^{3+} and found that the doping series $Ga_xZn_{1-x}Cu_3(OH)_6Cl_2$ should be stable in a broad range of Ga:Zn ratios (see Supplemental Information).

Electronic and magnetic properties

In the analysis of the electronic and magnetic properties we concentrate here on the hole-doped materials ($n = 2/3$, as defined in Fig. 2) where the Fermi level lies in the region of the flat band of the kagome lattice and a strong ferromagnetic instability is to be expected. Fig. 4a displays the fully relativistic non-spin-polarized electronic bandstructure of Li-herbertsmithite, where the parities of the three (dominantly Cu $d_{x^2-y^2}$) bands closest to the Fermi level are also indicated. Due to the bulk nature of the system, the ideal kagome flat band acquires some dispersion. Nonetheless, ferromagnetism is strongly favored. Indeed, total energy calculations of Li-herbertsmithite in various copper spin configurations give ferromagnetism as the ground state. Furthermore, parametrizing the Cu-Cu interactions by mapping DFT+U total energies to a spin-1/2 Heisenberg Hamiltonian shows a large ferromagnetic nearest neighbor exchange $J_1 = 544$ K and other couplings with magnitude smaller than $0.1J_1$. Using a mean-field approximation [48], we estimate a Curie temperature of $T_C \approx 1160$ K (see Supplemental Information for further details).

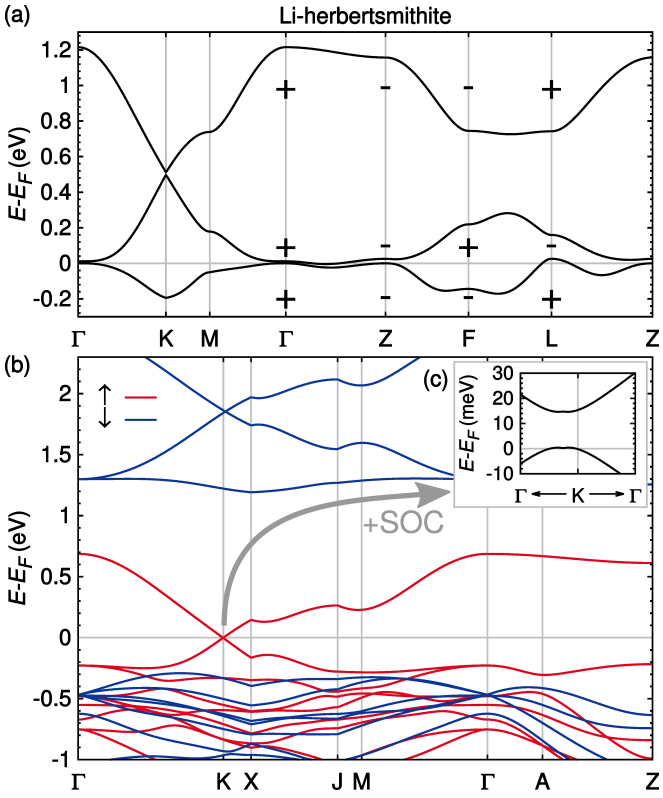

FIG. 4. (a) Fully relativistic non-spin-polarized bandstructure. Plus and minus signs denote the parities of the three bands closest to the Fermi level at eight inversion-symmetric points (Γ, $3\times F$, $3\times L$, Z) in the Brillouin zone. (b) FM bandstructure without SOC. The spin down channel is gapped, while the Dirac point of the spin up channel is located exactly at the Fermi level. The path through the Brillouin zone is shown in the Supplemental Information. (c) Fully relativistic FM bandstructure close to the Dirac point. SOC opens a gap.

Fig. 4b displays the non-relativistic ferromagnetic bandstructure obtained with the DFT+U functional. The Fermi level of the majority bands lies right at the Dirac pointand inclusion of spin orbit coupling opens a

gap of about 15 meV (see inset in Fig. 4). The Dirac point position is slightly displaced from K due to the finite coupling between the kagome layers, as has been observed previously in Ref. 12. The position of the Fermi level is understood by comparing the results to the spin-degenerate bandstructure shown in Fig. 2. The fully spin-polarized ferromagnetic state occurs at $n = 2/3$, therefore the spin-resolved fillings are $n_\uparrow = 2/3$ and $n_\downarrow = 0$. As a consequence, the bands of the majority spins resemble the non-spin-polarized case at $n = 4/3$ (where $n_\uparrow = n_\downarrow = 2/3$) and the minority spins are empty and gapped. The ferromagnetic instability places therefore the Fermi level of the up spin bands right at the Dirac point.

To show the presence of topologically protected edge states in doped herbertsmithite, we calculated the product of parity eigenvalues at eight inversion-symmetric points (see Fig. 4) in the Brillouin zone (Γ, $3 \times F$, $3 \times L$, Z) [49]. For all materials of the herbertsmithite family, topological numbers of the bands below the Dirac point are $\nu_0; (\nu_1, \nu_2, \nu_3) = 0; (111)$. These indices indicate that the system realizes a stack of two-dimensional topological insulators (so-called *weak* TI), which displays conducting states on a (001) surface [49], although the bulk bands are gapped by relativistic effects.

Note that non-trivial band topology is intrinsic to the perfect kagome lattice [21, 22] and no particular inversion of orbital weights is required unlike in most topological insulators [28, 50]. In real materials however, the kagome layer is embedded into a crystal, where non-trivial band-topology can be destroyed by additional hybridizations. We observed this case for instance in test calculations for modifications of the natural mineral barlowite, $A\mathrm{Cu_3(OH)_6FBr}$ [51, 52], which has a crystal structure similar to herbertsmithite with perfect kagome layers.

Demonstration of surface states

Having found non-trivial band-topology in the herbertsmithite system, we predict that hole-doped herbertsmithite shows a QAHE at $n = 2/3$ filling while electron-doped herbertsmithite shows a QSHE at $n = 4/3$ filling. For both cases we constructed realistic tight-binding models for the orbitals close to the Fermi energy and calculated the states on the (001) plane of semi-infinite interlayer-substituted herbertsmithite (for further details see Supplemental Information). The obtained spectral function $A(k, \omega)$ of the surface layer in chain termination is shown in Fig. 5, where the k-path is chosen perpendicular to the direction in which surface states propagate.

The hole-doped case clearly shows only one surface state of one spin species crossing the Fermi level (QAHE, see Fig. 5a), while the electron-doped case shows two surface states with opposite spin (QSHE, see Fig. 5b). The spectral function of the dual surface (triangles termination) has the same essential features (shown in the Supplemental Information). As we take into account realistic bandstructures, our spectral functions show additional structure away from the Fermi level compared to model calculations in next-neighbor approximation [21, 22].

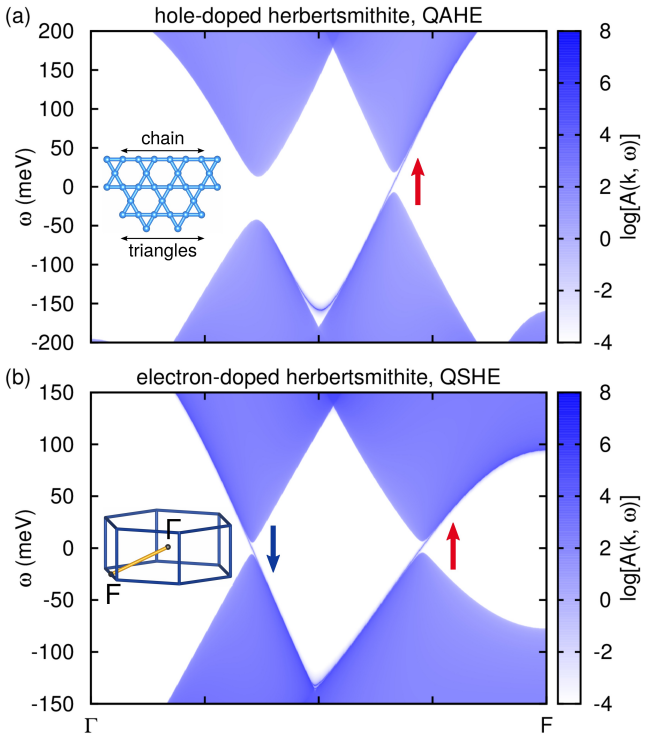

FIG. 5. Calculated surface states of substituted herbertsmithite. Spectral function on the (001) surface of (a) Li-herbertsmithite (hole-doped) and (b) Ga-herbertsmithite (electron-doped) calculated using Green's functions for the semi-infinite system. The arrows pointing upwards / downwards stand for the $m_j = +5/2$ and $-5/2$ states respectively. The inset of (a) shows the two possible terminations of the kagome lattice. The inset of (b) shows the path in the hexagonal Brillouin zone.

DISCUSSION

In this work we have presented a new generally applicable strategy for creating materials where the quantum anomalous Hall effect and the quantum spin Hall effect can be realized at affordable energy and temperature scales, based on existing kagome lattice Mott insulators.

For the quantum anomalous Hall effect we showed that if the Fermi level is placed into the kagome flat band, the reconstructed bands are fully spin-polarized and show a topologically non-trivial gap at the Fermi level with conducting surface states of only one spin species. We demonstrated our proposal by considering the kagome Mott insulator herbertsmithite. Although the kagome flat band is only nearly flat in the real system, a quantum anomalous Hall state with Curie temperature well above

1000 K is established upon chemical substitution. The correlated nature of the Cu 3*d* orbitals plays an important role for the existence of fully spin-polarized bands with a gap to the empty minority bands. As we have been dealing with 3*d* electrons, the calculated spin-orbit induced band gap is of the order of $15 - 20$ meV. Our scheme is applicable to 4*d* and 5*d* systems, where significantly larger spin-orbit band gaps are to be expected, while still preserving some correlation effects.

Electron doping of herbertsmithite up to the Dirac point yields, on the other hand, a topological insulator (QSHE). With the earlier prediction of superconductivity close to the Dirac point [12], the Ga_xZn_{1-x}-herbertsmithite system might present an interesting platform for building a topological quantum computer by locally controlling the Ga:Zn ratio.

Synthesis of such doped kagome systems may be a challenge. However, our calculations show a robust stability of the structures and correctly predict, for instance, that the Cd-substituted herbertsmithite distorts, as has been observed experimentally [53]. This gives some reassurance about the predictive power and actual realization of the phenomena proposed in the present work. Nevertheless, chemical doping may not be the only route to achieve hole or electron doping in herbertsmithite. In recent years a few alternative techniques have been very successful in doping Mott insulators like deposition of alkali ions [54] or gating the materials with ionic liquids [55, 56]. For instance, it has recently become possible to tune the critical temperature of La_2CuO_{4+x} thin films by gating the parent compound [57]. Following different doping routes may allow the realization of our predictions.

[1] Shores, M.P., Nytko, E.A., Bartlett, B.M. & Nocera, D.G. A Structurally Perfect S=1/2 Kagomé Antiferromagnet, *J. Am. Chem. Soc.* **127**, 13462-13463 (2005).

[2] Lee, S.-H. et al. Quantum-spin-liquid states in the two-dimensional kagome antiferromagnets $Zn_xCu_{4-x}(OD)_6Cl_2$. *Nat. Mater.* **6**, 853-857 (2007).

[3] de Vries, M.A., Kamenev, K.V., Kockelmann, W.A., Sanchez-Benitez, J. & Harrison, A. Magnetic Ground State of an Experimental $S = 1/2$ Kagome Antiferromagnet. *Phys. Rev. Lett.* **100**, 157205 (2008).

[4] Lee, P.A. An End to the Drought of Quantum Spin Liquids. *Science* **321**, 1306-1307 (2008).

[5] Balents, L. Spin liquids in frustrated magnets. *Nature* **464**, 199-208 (2010).

[6] Mendels, P. & Bert, F. Quantum Kagome Antiferromagnet $ZnCu_3(OH)_6Cl_2$. *J. Phys. Soc. Jpn.* **79**, 011001 (2010).

[7] Colman, R.H., Sinclair, A. & Willis, A.S. Comparisons between Haydeeite, α-$Cu_3Mg(OD)_6Cl_2$, and Kapellasite, α-$Cu_3Zn(OD)_6Cl_2$, Isostructural S = 1/2 Kagome Magnets. *Chem. Mater.* **22**, 5774-5779 (2010).

[8] Han, T.-H. et al. Fractionalized excitations in the spin-liquid state of a kagome-lattice antiferromagnet. *Nature* **492**, 406-410 (2012).

[9] Jeschke H.O., Salvat-Pujol, F. & Valentí, R. First-principles determination of Heisenberg Hamiltonian parameters for the spin-1/2 kagome antiferromagnet $ZnCu_3(OH)_6Cl_2$. *Phys. Rev. B* **88**, 075106 (2013).

[10] Li, Y. et al. Gapless quantum spin liquid in the S = 1/2 anisotropic kagome antiferromagnet $ZnCu_3(OH)_6SO_4$. *New J. Phys.* **16**, 093011 (2014).

[11] Bauer, B. et al. Chiral spin liquid and emergent anyons in a Kagome lattice Mott insulator. *Nat. Commun.* **5**, 5137 (2014).

[12] Mazin, I.I. et al. R. Thomale & R. Valentí, Theoretical prediction of a strongly correlated Dirac metal. *Nat. Commun.* **5**, 4261 (2014).

[13] Mook, A., Henk, J. & Mertig, I. Edge states in topological magnon insulators. *Phys. Rev. B* **90**, 024412 (2014).

[14] Pereiro, M. et al. Topological excitations in a kagome magnet. *Nat. Commun.* **5**, 4815 (2014).

[15] Chisnell, R. et al. Topological Magnon Bands in a Kagome Lattice Ferromagnet. *Phys. Rev. Lett.* **115**, 147201 (2015).

[16] Kane, C.L. & Mele, E.J. Quantum Spin Hall Effect in Graphene. *Phys. Rev. Lett.* **95**, 226801 (2005).

[17] Bernevig, B.A. & Zhang, S.-C. Quantum Spin Hall Effect. *Phys. Rev. Lett.* **96**, 106802 (2006).

[18] Hasan, M.Z. & Kane, C.L. Colloquium: Topological insulators. *Rev. Mod. Phys.* **82**, 3045-3067 (2010).

[19] Haldane, F.D.M. Model for a Quantum Hall Effect without Landau Levels: Condensed-Matter Realization of the "Parity Anomaly". *Phys. Rev. Lett.* **61**, 2015-2018 (1988).

[20] Liu, C.-X. Zhang, S.-C. & Qi, X.-L. The Quantum Anomalous Hall Effect: Theory and Experiment. *Annu. Rev. Condens. Matter Phys.* **7**, 301-321 (2016).

[21] Wang, Z. & Zhang, P. Quantum spin Hall effect and spin-charge separation in a kagomé lattice. *New J. Phys.* **12**, 043055 (2010).

[22] Zhang, Z.-Y. The quantum anomalous Hall effect in kagomé lattices. *J. Phys.: Condens. Matter* **23**, 365801 (2011).

[23] Fu, L. & Kane, C. L. Superconducting Proximity Effect and Majorana Fermions at the Surface of a Topological Insulator. *Phys. Rev. Lett.* **100**, 096407 (2008).

[24] Wilczek, F. Majorana returns. *Nat. Phys.* **5**, 614-618 (2009).

[25] Das Sarma, S. Freedman, M. & Nayak, C. Majorana zero modes and topological quantum computation. *npj Quantum Information* **1**, 15001 (2015).

[26] He, K. The Quantum Hall Effect Gets More Practical. *Physics* **8**, 41 (2015).

[27] Weng, H. Yu, R. Hu, X. Dai, X. & Fang, Z. Quantum anomalous Hall effect and related topological electronic states. *Adv. Phys.* **64**, 227-282 (2015).

[28] Yu, R. et al. Quantized Anomalous Hall Effect in Magnetic Topological Insulators. *Science* **329**, 61-64 (2010).

[29] Chang, C.-Z. et al. Experimental Observation of the Quantum Anomalous Hall Effect in a Magnetic Topological Insulator. *Science* **340**, 167-170 (2013).

[30] Garrity, K.F. & Vanderbilt, D. Chern Insulators from Heavy Atoms on Magnetic Substrates. *Phys. Rev. Lett.* **110**, 116802 (2013).

[31] Wu, S.-C. Shang, G. & Yan, B. Prediction of Near-Room-Temperature Quantum Anomalous Hall Effect on Honeycomb Materials. *Phys. Rev. Lett.* **113**, 256401 (2014).

[32] Xu, G. Lian, B. & Zhang, S.-C. Intrinsic Quantum Anomalous Hall effect in Kagome lattice $Cs_2LiMn_3F_{12}$. *Phys. Rev. Lett.* **115**, 186802 (2015).

[33] Wang, Z.F. Liu Z. & Liu, F. Quantum Anomalous Hall Effect in 2D Organic Topological Insulators. *Phys. Rev. Lett.* **110**, 196801 (2013).

[34] Yamada, M.G. et al. First-Principles Design of a Half-Filled Flat Band of the Kagome Lattice in Two-Dimensional Metal-Organic Frameworks. arXiv:1510.00164 (unpublished).

[35] Ohashi, T. Kawakami, N. & Tsunetsugu, H. Mott Transition in Kagomé Lattice Hubbard Model. *Phys. Rev. Lett.* **97**, 066401 (2006).

[36] Tang, E. Mei, J.-W. & Wen, X.-G. High-Temperature Fractional Quantum Hall States. *Phys. Rev. Lett.* **106**, 236802 (2011).

[37] Hanisch, T. Uhrig, G. & Müller-Hartmann, E. Lattice dependence of saturated ferromagnetism in the Hubbard model. *Phys. Rev. B* **56**, 13960-13982 (1997).

[38] Blöchl, P.E. Projector augmented-wave method. *Phys. Rev. B* **50**, 17953-17979 (1994).

[39] Enkovaara, J. et al. Electronic structure calculations with GPAW: a real-space implementation of the projector augmented-wave method. *J. Phys.: Condens. Matter* **22**, 253202 (2010).

[40] Perdew, J.P. Burke, K. & Ernzerhof, M. Generalized Gradient Approximation Made Simple. *Phys. Rev. Lett.* **77**, 3865-3868 (1996).

[41] Koepernik, K. & Eschrig, H. Full-potential nonorthogonal local-orbital minimum-basis band-structure scheme. *Phys. Rev. B* **59**, 1743-1757 (1999).

[42] Liechtenstein, A.I., Anisimov, V.I. & Zaanen, J. Density-functional theory and strong interactions: Orbital ordering in Mott-Hubbard insulators. *Phys. Rev. B* **52**, R5467-R5470 (1995).

[43] Eschrig, H. & Koepernik, K. Tight-binding models for the iron-based superconductors. *Phys. Rev. B* **80**, 104503 (2009).

[44] López Sancho, M.P. López Sancho, J.M. & Rubio, J. Quick iterative scheme for the calculation of transfer matrices: application to Mo(100). *J. Phys. F: Met. Phys.* **14**, 1205-1215 (1984).

[45] López Sancho, M.P., López Sancho, J.M. & Rubio, J. Highly convergent schemes for the calculation of bulk and surface Green functions. *J. Phys. F: Met. Phys.* **15**, 851-858 (1985).

[46] Dai, X. Hughes, T.L., Qi, X.-L., Fang, Z. & Zhang, S.-C. Helical edge and surface states in HgTe quantum wells and bulk insulators. *Phys. Rev. B* **77**, 125319 (2008).

[47] Shannon, R.D. Revised Effective Ionic Radii and Systematic Studies of Interatomic Dinstances in Halides and Chalcogenides. *Acta Cryst. A* **32**, 751-767 (1976).

[48] Blundell, S. *Magnetism in Condensed Matter* (Oxford University Press, Oxford, 2010).

[49] Fu, L. & Kane, C.L. Topological insulators with inversion symmetry. *Phys. Rev. B* **76**, 045302 (2007).

[50] Zhou, L. et al. New Family of Quantum Spin Hall Insulators in Two-dimensional Transition-Metal Halide with Large Nontrivial Band Gaps. *Nano Lett.* **15**, 7867-7872 (2015).

[51] Han, T.-H., Singleton, J. & Schlueter, J.A. Barlowite: A Spin-1/2 Antiferromagnet with a Geometrically Perfect Kagome Motif. *Phys. Rev. Lett.* **113**, 227203 (2014).

[52] Jeschke, H.O. et al. Barlowite as a canted antiferromagnet: Theory and experiment. *Phys. Rev. B* **92**, 094417 (2015).

[53] McQueen, T.M. et al. $CdCu_3(OH)_6Cl_2$: A new layered hydroxide chloride. *J. Solid State Chem.* **184**, 3319-3323 (2011).

[54] Kim, Y.K. et al. Fermi arcs in a doped pseudospin-1/2 Heisenberg antiferromagnet. *Science* **345**, 187-190 (2014).

[55] Ye, J.T. et al. Liquid-gated interface superconductivity on an atomically flat film. *Nature Mater.* **9**, 125-128 (2010).

[56] Nakano, M. et al. Collective bulk carrier delocalization driven by electrostatic surface charge accumulation. *Nature* **487**, 459-462 (2012).

[57] Kinney, J., Garcia-Barriocanal, J. & Goldman, A.M. Homes scaling in ionic liquid gated La_2CuO_{4+x} thin film, *Phys. Rev. B* **92**, 100505(R) (2015).

ACKNOWLEDGMENTS

The authors thank Kira Riedl, Milan Tomić, Bernd Wolf, Pascal Puphal, Cornelius Krellner, Hans Boschker, Jochen Mannhart, Martin Jansen, Claudia Felser, Flavio Yair Bruno and Alberto Rivera Calzada for fruitful discussions. This work was supported by the German Research Foundation (Deutsche Forschungsgemeinschaft) through grant SFB/TR 49. RV was supported in part by Kavli Institute for Theoretical Physics at the University of California, Santa Barbara under National Science Foundation grant No. PHY11-25915.

AUTHOR CONTRIBUTIONS

DG and HOJ performed the calculations. RV supervised the project. All authors participated in the discussion and wrote the manuscript.

ADDITIONAL INFORMATION

Competing financial interests: The authors declare that they have no competing financial interests.

Supplemental Material: Prospect of quantum anomalous Hall and quantum spin Hall effect in doped kagome lattice Mott insulators

Daniel Guterding,* Harald O. Jeschke, and Roser Valentí
Institut für Theoretische Physik, Goethe-Universität Frankfurt, Max-von-Laue-Straße 1, 60438 Frankfurt am Main, Germany

I. FORMATION AND DOPING ENERGIES

Total energies were evaluated using *ab-initio* density functional theory (DFT) calculations within an all-electron full-potential local orbital (FPLO) [1] basis. For the exchange-correlation functional we employ the generalized gradient approximation (GGA) [2]. Total energies were extracted from calculations converged using 8^3 k-point grids.

Experimental and hypothetical crystal structures were fully relaxed using the projector augmented wave (PAW) method [3] implemented in GPAW [4] with a plane-wave cutoff of 1000 eV and the GGA exchange-correlation functional [2]. We optimized the stoichiometric structures of herbertsmithite-based compounds using 6^3 k-points (4^3 k-points for non-stoichiometric structures) until forces were below $10\,\mathrm{meV/Å}$.

Hypothetical crystal structures were prepared starting from the experimental crystal structure of herbertsmithite [5], substituting zinc (Zn) atoms between the copper kagome layers by monovalent A=Li, Na (hole-doping) and trivalent Al, Ga, In, Sc, Y (electron-doping). We refer to these compounds as A-herbertsmithite, $A\mathrm{Cu_3(OH)_6Cl_2}$ (case 1) and estimate their stability by comparison to clinoatacamite [$\mathrm{Cu_2(OH)_3Cl}$]. We directly compare energies of A-substituted materials, where the dopant sits in the interlayer site versus structures where it occupied a kagome site (case 2, see Fig. 3 in main paper). To analyze the phase stability, we also evaluate total energies of $3\times1\times1$ supercell structures, where either one of the A-sites is vacant [$A_{0.66}\mathrm{Cu_3(OH)_6Cl_2}$, case 3] or occupied by a Cu impurity [$A_{0.66}\mathrm{Cu_{3.33}(OH)_6Cl_2}$, case 4].

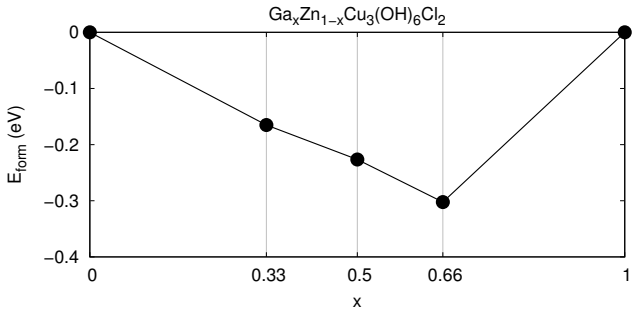

FIG. 1. Formation energies of the $\mathrm{Ga}_x\mathrm{Zn}_{1-x}\mathrm{Cu_3(OH)_6Cl_2}$ doping series. Lines are guides to the eye.

In order to determine whether the presence of excess copper in the synthesis process makes the formation of clinoatacamite favorable compared to $A\mathrm{Cu_3(OH)_6Cl_2}$, we compare the total energies of Cu in a copper crystal plus the energy of $A\mathrm{Cu_3(OH)_6Cl_2}$ to the total energy of A in a crystal of substance A plus the total energy of clinoatacamite. Proper normalization of total energies to formula units is taken into account. The calculated energy difference determines whether the formation of metallic patches of substance A is energetically favourable compared to forming A-substituted herbertsmithite. The formation energy for this case is defined as

$$E_{\mathrm{form}} = E_{\mathrm{Cu}} + E_{\mathrm{AH}} - (E_A + E_{\mathrm{C}})\,, \qquad (1)$$

where E_{A} refers to the pure crystalline metal A, E_{AH} to A-herbertsmithite and E_{C} to clinoatacamite. As all total energies are negative, a negative formation energy signals stability of the target compound $A\mathrm{Cu_3(OH)_6Cl_2}$. As a consistency check, we also prepared a structure with copper on the interlayer site so that the chemical formula is identical to clinoatacamite. For this structure, we find a positive formation energy. Therefore, hypothetical Cu-herbertsmithite is unstable with respect to the formation of clinoatacamite, as expected.

For the formation energy of impurity or vacancy structures, we use

$$E_{\mathrm{form}} = y\cdot E_{\mathrm{Cu}} + E_{\mathrm{AH}} - (x\cdot E_A + E_{\mathrm{AHM}})\,, \qquad (2)$$

where E_{AHM} is the total energy of the compound $A_{1-x}\mathrm{Cu}_{3+y}\mathrm{(OH)_6Cl_2}$.

Formation energies for modifications of herbertsmithite are shown in Table I. As all calculated energy differences are negative, formation of A-herbertsmithite is always favorable compared to formation of clinoatacamite. All proposed modifications are robust against formation of vacancies or copper impurities on the (interlayer) A-site.

The doping energies shown in Fig. 3 of the main paper are computed from energy differences between structures with dopant atoms occupying the interlayer sites and structures with dopant atoms on a kagome site (case 2). The values for the doping energies are given in Table I, together with ionic radii taken from Ref. [6].

Having established the stability of stoichiometric compounds, we investigate the solid solution of Zn and Ga

* guterding@itp.uni-frankfurt.de

TABLE I. Calculated formation and doping energies for substituted herbertsmithite. Energies are given in eV (electron volts) per formula unit of A-substituted herbertsmithite $A\mathrm{Cu_3(OH)_6Cl_2}$ (A = Li, Na, Zn, Cd, Sc, Y, Al, Ga, In). Negative values signal stability of the stoichiometric compound against the formation of clinoatacamite (case 1), doping into the kagome layer (case 2, see Fig. 3 in main paper), vacancies on the interlayer site (case 3) and impurities on the interlayer site (case 4). Ionic radii in coordination number 6 are taken from Ref. [6]. In this configuration Cu^{2+} has an ionic radius of 72 pm.

case	A-herbertsmithite, $A=$	Li^{1+}	Na^{1+}	Zn^{2+}	Cd^{2+}	Sc^{3+}	Y^{3+}	Al^{3+}	Ga^{3+}	In^{3+}
1	$A\mathrm{Cu_3(OH)_6Cl_2}$	-2.660	-2.517	-2.082	-1.461	-7.300	-7.144	-6.257	-2.939	-3.080
2	$A\mathrm{Cu_3(OH)_6Cl_2}$	-0.041	+0.257	-0.261	+0.128	-0.372	+0.043	-1.101	-0.736	-0.203
3	$A_{0.66}\mathrm{Cu_3(OH)_6Cl_2}$	-0.847	-0.735	-0.694	n/a	-2.481	-2.398	-2.141	-1.176	-1.062
4	$A_{0.66}\mathrm{Cu_{3.33}(OH)_6Cl_2}$	-1.497	-1.350	-1.321	n/a	-3.019	-2.878	-2.659	-1.711	-1.585
	ionic radius in pm	76	102	74	95	75	90	54	62	80

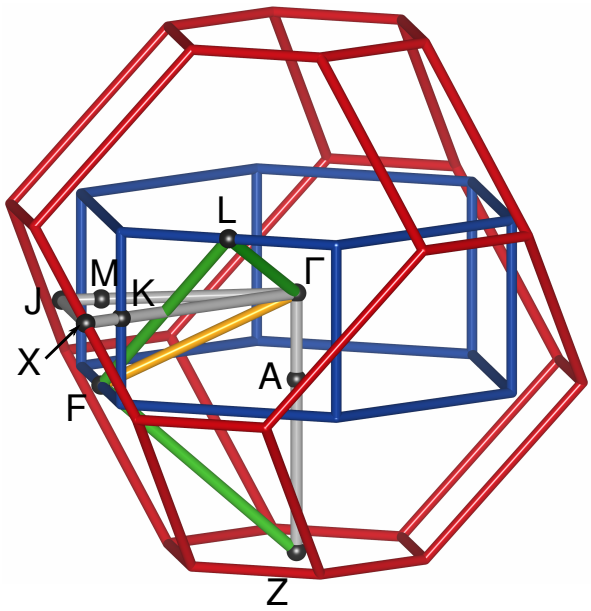

FIG. 2. Brillouin zone of herbertsmithite with high-symmetry points. The space group is $R\bar{3}m$. The path conventionally used for showing the bandstructure of herbertsmithite is indicated in grey. A path comprising the time-reversal invariant points is shown in green. The path on which surface states were calculated is shown in yellow.

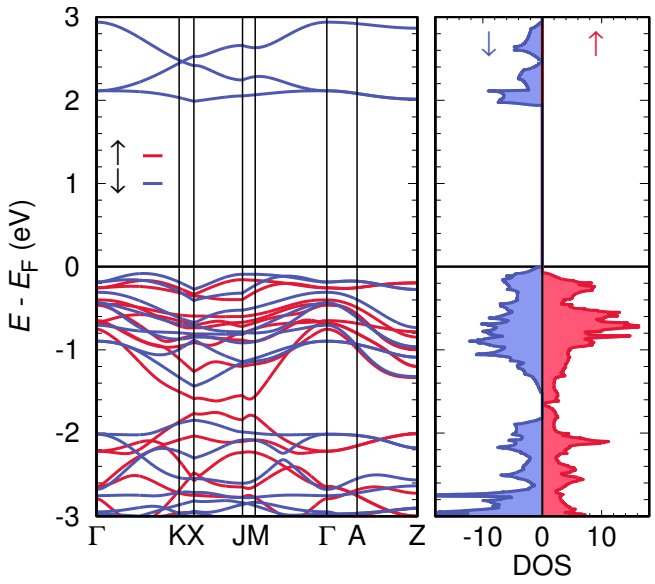

FIG. 3. Spin-polarized electronic bandstructure of herbertsmithite in ferromagnetic spin-configuration calculated from DFT+U. The interaction parameters on the Cu 3d shell are U = 6 eV and Hund's rule coupling J_H = 1 eV. A gap of about 2 eV is opened at the Fermi level due to electron-electron interactions.

dopants. To accomodate non-integer dopant concentrations, we use $2\times1\times1$ and $3\times1\times1$ super cells. The formation energy of the target compound having total energy E_T is defined as

$$E_\mathrm{form} = E_\mathrm{T} + x\cdot(E_\mathrm{Zn} - E_\mathrm{Ga}) - (1-x)\cdot E_\mathrm{ZnH} - x\cdot E_\mathrm{GaH}, \quad (3)$$

where E_ZnH refers to herbertsmithite and E_GaH to Gallium-substituted herbertsmithite. Note that as a reference energy here we use $(1-x)\cdot E_\mathrm{ZnH} + x\cdot E_\mathrm{GaH}$, which is the energy that one obtains if the solid solution were to dissociate spontaneously into herbertsmithite and Ga-substituted herbertsmithite. Therefore, formation energies are negative if the solid solution is stable against phase separation. Our results show that the solid solution $\mathrm{Ga}_x\mathrm{Zn}_{1-x}\mathrm{Cu_3(OH)_6Cl_2}$ should exist in a broad range of doping ratios (Fig. 1).

II. DETAILS ON PREPARATION OF HYPOTHETICAL CRYSTAL STRUCTURES

For all cases discussed in the previous section, crystal structures had to be prepared from a stoichiometric structure of herbertsmithite [5]. We started from the rhombohedral unit cell of space group $R\bar{3}m$, containing one formula unit. After reducing symmetry to space group $P1$, herbertsmithite allows for only one possibility to arrange dopant atoms or defects for all compositions investigated here, if the smallest possible supercell is considered.

Fig. 2 shows the Brillouin zone with high-symmetry points for materials based on herbertsmithite.

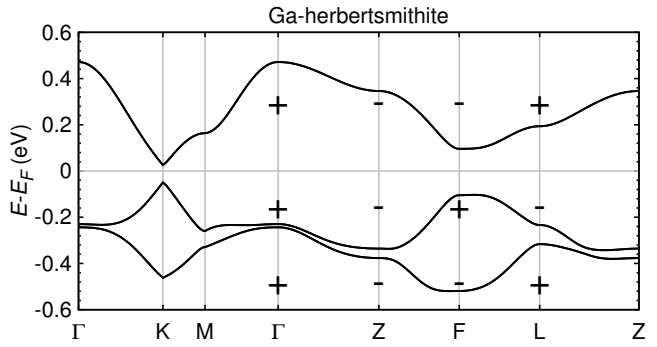

FIG. 4. Fully relativistic bandstructure of Ga-herbertsmithite. Plus and minus signs denote the parities of the three bands closest to the Fermi level at eight inversion-symmetric points (Γ, $3\times F$, $3\times L$, Z) in the Brillouin zone. In Ga-herbertsmithite the bandstructure is more three-dimensional than in Li-herbertsmithite, which leads to a substantial displacement of the Dirac point from the high-symmetry point K. In turn the apparent gap at K is exaggerated.

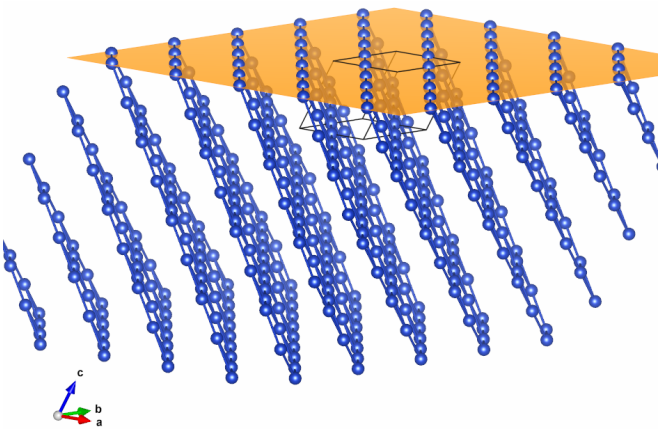

FIG. 5. (001) surface of herbertsmithite (shown as orange colored plane). Here, we used the predicted structure of Li-herbertsmithite. Ions other than Cu are omitted for clarity. The rhombohedral unit cell is shown in black. Note how all kagome layers are terminated with chains of copper ions at the surface.

III. BANDSTRUCTURE OF HERBERTSMITHITE IN FERROMAGNETIC SPIN-CONFIGURATION

Herbertsmithite is an antiferromagnetic Mott insulator with possible quantum spin liquid ground state. Although density functional theory cannot describe such a paramagnetic ground state with large fluctuating moments, a DFT+U calculation for the most simple ordered magnetic configuration (ferromagnetic) already reproduces the insulating ground state of herbertsmithite with a large band gap of about 2 eV (see Fig. 3).

IV. BANDSTRUCTURE AND TOPOLOGICAL PROPERTIES OF ELECTRON-DOPED HERBERTSMITHITE

We also analysed the bandstructure and topological properties of electron-doped herbertsmithite. As an example, in Fig. 4 we show the fully relativistic non-spin-polarized electronic bandstructure of Ga-herbertsmithite, where the parities of the three (dominantly Cu $d_{x^2-y^2}$) bands closest to the Fermi level are indicated. Ga-herbertsmithite is more three-dimensional than Li-herbertsmithite. Therefore, the Dirac point is displace from K, which exaggerates the gap at K. At the Dirac point the gap magnitude is the same as in Li-herbertsmithite.

The paritiy eigenvalues of the bands closest to the Fermi level are the same as in all other compounds derived from herbertsmithite that we predict to be stable. That means, topological numbers of the bands below the Dirac point are $\nu_0;(\nu_1,\nu_2,\nu_3)=0;(111)$.

V. FORMALISM FOR COMPUTING SURFACE STATES

We use the Green's function method for the semi-infinite system [7–9] to calculate the states on the (001) surface of interlayer substituted herbertsmithite. In this scheme, the crystal must be partitioned into so-called principal layers parallel to the surface of interest. The Hamiltonian within the principal layer is denoted as H_0, while the coupling between neighboring principal layers is denoted as C. Note that only hoppings with components in direction either negative or positive perpendicular to the surface must be included into C. The corresponding couplings in the reverse direction are taken into account in the formalism by the adjoint matrix $C^\dagger$.

The surface Green's function of a system consisting of N principal layers can be written as

$$G_{ij}^{(N)}(\omega)=\left[\left(\omega-H_0-CG^{(N-1)}C^\dagger\right)^{-1}\right]_{ij}. \quad (4)$$

The initial condition is

$$G_{ij}^{(1)}(\omega)=(\omega-H_0)_{ij}^{-1}. \quad (5)$$

Indices i,j denote combined site, orbital and spin variables. The Green's function of the dual surface can be calculated by iterating

$$G_{ij}^{(N)}(\omega)=\left[\left(\omega-H_0-C^\dagger G^{(N-1)}C\right)^{-1}\right]_{ij}. \quad (6)$$

As we use Green's functions on the real-frequency axis, an artificial imaginary part must be added to ensure numerical convergence. To this end, we transform $\omega\to\omega+i\eta$ with $\eta=10^{-5}$ eV in the equations above.

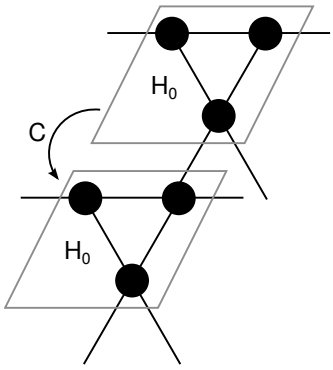

FIG. 6. Schematic partitioning of the tight-binding Hamiltonian into layers parallel to the surface. The principal layer is described by Hamiltonian H_0, while C contains hopping elements connecting two adjacent principal layers. In the real herbertsmithite system longer range hoppings are included and two kagome layers belong to one unit cell. For comparison, see Fig. 5.

Although the method in principle allows for the treatment of semi-infinite systems, the numerical iteration of Eq. (4) or (6) has to be stopped with a finite number of layers. We use $N = 10^5$.

VI. (001) SURFACE OF HERBERTSMITHITE

In the main paper we presented topological invariants $\nu_0; (\nu_1, \nu_2, \nu_3) = 0; (111)$ for the herbertsmithite system. According to Ref. [10], a material with those topological invariants displays conducting states on a (001) surface. The orientation of this lattice plane refers to the unit cell in rhombohedral setting of space group $R\bar{3}m$. The (001) surface of Li-herbertsmithite is shown in Fig. 5. Note how the Cu ions at the surface are arranged in chains, with all kagome layers terminated equivalently.

The unit cell of (substituted) herbertsmithite contains in total three Cu ions. These three ions comprise the minimal model of the herbertsmithite material. In the (001) surface geometry we use, two of the ions are at the surface and one is below the surface. The minimal principal layer therefore comprises Cu ions at different heights within the unit cell. This complicates the partitioning of hopping elements into matrices H_0 and C needed for the Green's function method. The situation is depicted in Fig. 6.

As mentioned in the main paper, and obvious from Fig. 6, the semi-infinite system can be built up either in positive or negative direction perpendicular to the surface. In the kagome lattice this results in an edge termination with either chains or triangles. The case of chains is presented in the main paper. For the dual surface (triangles termination) one obtains a spectral function with equivalent features (see Fig. 7) from Eq. (6).

Both in the main paper and in the supplement we show the spectral function $A(k, \omega)$ only in positive k-direction

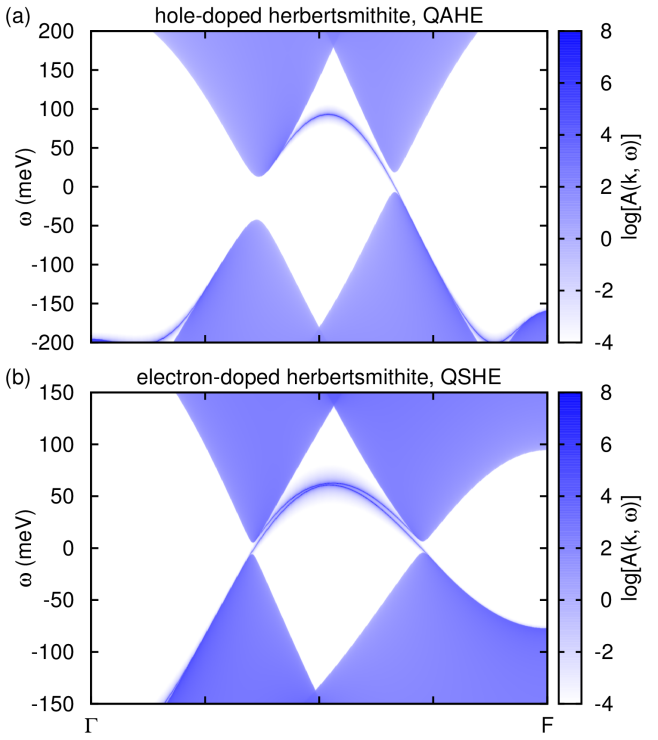

FIG. 7. Calculated states on the dual surface of substituted herbertsmithite. Spectral function on the (001) surface of (a) Li-herbertsmithite (hole-doped) and (b) Ga-herbertsmithite (electron-doped) calculated using Green's functions for the semi-infinite system. The kagome layers are terminated with triangles.

within the k_x-k_y-plane. As can bee seen from Fig. 5, the surface unit cell of (001) herbertsmithite contains two chains of Cu ions. The surface is mirror symmetric with respect to the k_x and the k_y-direction. Therefore, the symmetry equivalent edge states of the second kagome layer appear in negative k-direction.

VII. DETERMINATION OF HEISENBERG HAMILTONIAN PARAMETERS

Based on the theoretically predicted structures of Li-herbertsmithite (see Table II, Fig. 8a), we use density functional theory calculations to determine the most important couplings of the Heisenberg Hamiltonian. We use the all electron full potential local orbital (FPLO) code [1] with a generalized gradient approximation [2] exchange and correlation functional and correct for the strong correlations on the Cu^{2+} $3d$ orbitals using GGA+U [11].

The results for $LiCu_3(OH)_6Cl_2$ are given in Table III. The calculation was performed with a $\sqrt{2} \times \sqrt{2} \times 2$ supercell of the rhombohedral primitive cell of Li-herbertsmithite. With $P1$ symmetry, this cell contains four formula units, *i.e.* twelve inequivalent Cu sites. This

TABLE II. Predicted structural parameters for Li-herbertsmithite [$LiCu_3(OH)_6Cl_2$]. ($R\bar{3}m$ space group, $a = 6.96433$ Å, $c = 13.78483$ Å, $Z = 3$)

Atom	Site	x	y	z
Cu	$9d$	1/2	0	1/2
Li	$3a$	0	0	0
O	$18h$	-0.208833	0.208833	0.447033
H	$18h$	-0.131973	0.131973	0.420633
Cl	$6c$	0	0	0.328170

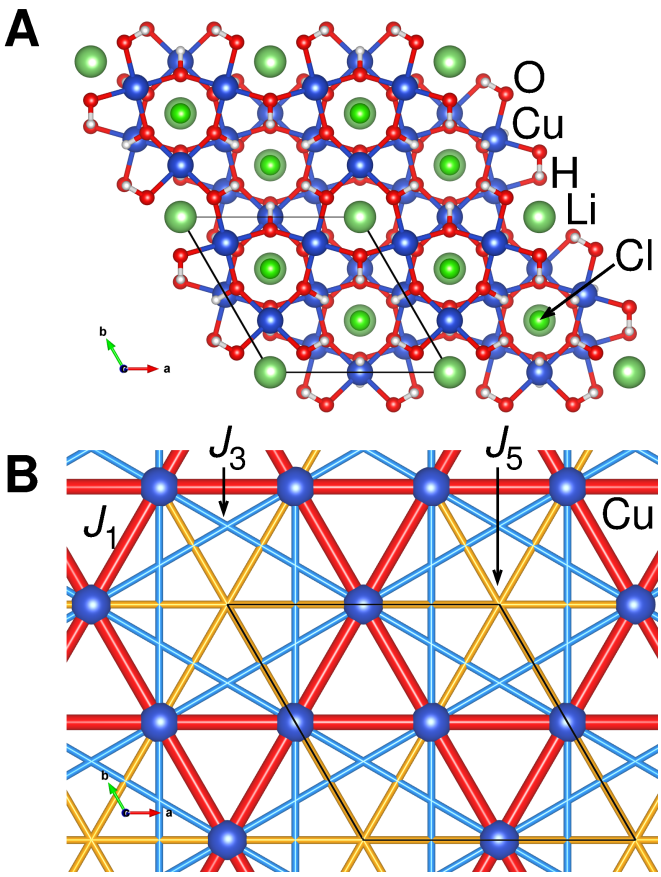

FIG. 8. Predicted crystal structure and exchange paths in Li-herbertsmithite. (a) View of the Li-herbertsmithite structure along c direction (in hexagonal setting of the $R\bar{3}m$ space group). (b) Detail of the $LiCu_3(OH)_6Cl_2$ unit cell with the first three inplane exchange paths between Cu^{2+} ions. Other ions are omitted for clarity.

TABLE III. Calculated exchange couplings for predicted Li-herbertsmithite, $LiCu_3(OH)_6Cl_2$. A GGA+U functional with $J_H = 1$ eV and the two listed U values was used in combination with fully localized limit double counting correction.

U (eV)	J_1 (K)	J_2 (K)	J_3 (K)	J_5 (K)	J_6 (K)
6.0	-544(29)	7(15)	39(24)	-50(13)	2(8)
8.0	-332(32)	-13(16)	-11(27)	-75(20)	1(8)

allows for 171 out of 4096 unique spin configurations, and the data in Table III are based on fits to total energies for about 30 of these configurations. The exchange couplings are given assuming $S = 1/2$. However, due to the changed filling of the Cu bands, the moments in the calculation are reduced from 1 μ_B to, on average, about 0.67 μ_B. The relevant exchange paths are visualized in Fig. 8b. Based on previous work [12], we consider the GGA+U functional with $U = 6$ eV, $J_H = 1$ eV most relevant for Cu in the square planar environment as realized in herbertsmithite type crystals.

VIII. ESTIMATE FOR THE CURIE TEMPERATURE

We estimate the Curie temperature T_C from a simple Weiss mean-field formula [13]. For $3d$ transition metals, in this approximation the Curie temperature is given by Eq. (7), where z_i is the coordination number and J_i are the exchange couplings in Kelvin ($U = 6$ eV), taken from Table III.

$$T_C = -\frac{2}{3}S(S+1)\sum_i z_i J_i \qquad (7)$$

We obtain $T_C = 1160$ K, where we took into account $i = \{1, 3, 5\}$ with $z_i = \{4, 4, 6\}$. Instead of the spin-1/2 model used here, it is also conceivable to parametrize the Heisenberg model with DFT effective moments for S, which would result in a higher value for T_C.

[1] K. Koepernik and H. Eschrig, *Full-potential nonorthogonal local-orbital minimum-basis band-structure scheme*, Phys. Rev. B **59**, 1743 (1999); http://www.FPLO.de

[2] J. P. Perdew, K. Burke, and M. Ernzerhof, *Generalized Gradient Approximation Made Simple*, Phys. Rev. Lett. **77**, 3865 (1996).

[3] P. E. Blöchl, *Projector augmented-wave method*, Phys. Rev. B **50**, 17953 (1994).

[4] J. Enkovaara, C. Rostgaard, J. J. Mortensen *et al.*, *Electronic structure calculations with GPAW: a real-space implementation of the projector augmented-wave method*, J. Phys.: Condens. Matter **22**, 253202 (2010); https://wiki.fysik.dtu.dk/gpaw

[5] M. P. Shores, E. A. Nytko, B. M. Bartlett, and D. G. Nocera, *A Structurally Perfect S=1/2 Kagomé Antiferromagnet*, J. Am. Chem. Soc. **127**, 13462 (2005).

[6] R. D. Shannon, *Revised Effective Ionic Radii and Systematic Studies of Interatomic Dinstances in Halides and Chalcogenides*, Acta Cryst. A **32**, 751 (1976).

[7] M. P. López Sancho, J. M. López Sancho, and J. Rubio, *Quick iterative scheme for the calculation of transfer matrices: application to Mo(100)*, J. Phys. F: Met. Phys. **14**, 1205 (1984).

[8] M. P. López Sancho, J. M. López Sancho, and J. Rubio, *Highly convergent schemes for the calculation of bulk and surface Green functions*, J. Phys. F: Met. Phys. **15**, 851 (1985).

[9] X. Dai, T. L. Hughes, X.-L. Qi, Z. Fang, and S.-C. Zhang, *Helical edge and surface states in HgTe quantum wells and bulk insulators*, Phys. Rev. B **77**, 125319 (2008).

[10] L. Fu and C. L. Kane, *Topological insulators with inversion symmetry*, Phys. Rev. B **76**, 045302 (2007).

[11] A. I. Liechtenstein, V. I. Anisimov, and J. Zaanen, *Density-functional theory and strong interactions: Orbital ordering in Mott-Hubbard insulators*, Phys. Rev. B **52**, R5467(R) (1995).

[12] H. O. Jeschke, F. Salvat-Pujol, and R. Valentí, *First-principles determination of Heisenberg Hamiltonian parameters for the spin-1/2 kagome antiferromagnet* $ZnCu_3(OH)_6Cl_2$, Phys. Rev. B **88**, 075106 (2013).

[13] S. Blundell, *Magnetism in Condensed Matter* (Oxford University Press, Oxford, 2010).